Efficiency Analysis of a combined PEFC and Bioethanol-Solar-Reforming System for Individual Houses

Shin-ya OBARA

Professor
Department of Electrical and Electronic Engineering, Kitami Institute of Technology
165 Koen-cho, Kitami, Hokkaido 090-8507, Japan
Phone/FAX +81-157-26-9262
E-mail: obara@mail.kitami-it.ac.jp

Abstract

In this research, the development of a bioethanol reforming system for fuel cells (FBSR: fuel cell with bioethanol steam reforming) using sunlight as a heat source was investigated. The system was investigated using the experimental result of catalyst performance, and numerical analysis. If ethanol purity is high, the production method of the bioethanol used for the proposal system will not be limited. The overall efficiency of the production of electricity and heat power of this system was determined by examining its thermal output characteristic. The FBSR was introduced into standard individual houses in Sapporo, Japan for analysis. The amount of hydrogen production, the production-of-electricity characteristic, and the thermal output characteristic were examined using meteorological data on representative days in March and August. Compared with the representative day in March (28.0 MJ/Day), the solar radiation of the representative day in August (37.0 MJ/Day) is large. However, the amount of solar radiation fluctuation of the representative day in August in this analysis is large compared with the representative day in March. It depends for the overall efficiency of the system on the amount of solar radiation fluctuation rather than the amount of solar radiation. As a result, the overall efficiency of the system, defined as the rate of power and heat output compared to the amount of solar heat collected, was calculated to be 47.4 % and 41.9 % on the representative days in March and August, respectively.

Keywords: Solar Reforming, Bioethanol, PEFC, Hydrogen Production

1. Introduction

The development of a distributed power supply with limited greenhouse gas emission is a global issue of current interest and importance. PEFCs (polymer electrolyte fuel cells) are one candidate for a clean, distributed power supply. However, the environmental impact of fuel cells changes greatly depending on the method of hydrogen production. For example, a large quantity of CO_2 is discharged when using reforming methods that employ fossil fuels. Alternatively, a fuel cell system that uses the heat of a small solar collector for the steam reforming of bioethanol, a bioethanol reforming system for fuel cells (FBSR system), has been examined [1-3]. Furthermore, there are researches on much hydrogen production technology using solar energy currently (for example, [4-7]). In this research, we have investigated the characteristics of the reformed gas production [1], the production-of-electricity characteristic of the FBSR using the weather forecast [2, 3], and the

relationship between solar insolation with fluctuation and a production-of-electricity characteristic [8]. This paper continues these reports. The main objectives of this paper are to compare the efficiency of the overall efficiency of the FBSR, and competition technology. If the overall efficiency of the proposal system is higher than competition technology, the trial production of the proposal system is effective. Moreover, in this study, fluctuation of solar radiation was taken into consideration to the reaction rate of steam reforming. There is no example of investigation of the solar reforming with solar radiation fluctuation in the past. The conversion rate of the reforming reaction of ethanol/water vapor is influenced by the temperature of a catalyst layer and the space velocity of a process gas [8]. A pellet type reforming catalyst is installed in the reactor of the FBSR. Reformed gas with a high hydrogen composition is outputted by supplying ethanol/water vapor to the reactor under the control of reactor temperature. However, because the heat source of a reactor is sunlight, the conversion rate of the fuel is affected by weather. Unsteady heat transfer analysis was introduced into the catalyst layer in a previous examination [8]. From this analysis, the transient response characteristic concerning the temperature distribution in the catalyst layer and composition of the process gas were investigated. As a result, under the weather conditions with high levels of solar radiation fluctuation over a short time, it became clear that a reforming reaction was not sufficient under the effect of a response delay. Moreover, it clarified the generation efficiency of the FBSR when taking into consideration the transient response characteristic of the reforming reaction. This paper investigates the thermal output characteristic of the FBSR. The overall efficiency of the system is clarified in consideration of these results and the result of the last report. It is the objective of this paper to highlight the differences between the FBSR and competing technologies, such as photovoltaic cells.

2. Material and Method

2.1 System block diagram

Figure 1 (a) is a block diagram of the fuel cell system with a bioethanol solar reforming system (FBSR). The solar tracking system is introduced into two solar collectors. Moreover, each collector's collecting area is nearly 1.0 m^2. Bioethanol for the boiler and the bioethanol solution for reforming are contained in a fuel tank. The S/C (molar ratio of steam to ethanol [9]) of the bioethanol solution for reforming is 3.0. Two parabolic mirrors (solar collector) with a solar tracking system are introduced into the FBSR. The heat for fuel evaporation is condensed in solar collector A while the heat for reforming of the fuel vapor is condensed in solar collector B.

2.2 Fuel and reformed gas system

(1) Flow of fuel and reformed gas

The fuel for reforming (bioethanol solution) is supplied to the vaporizer installed in solar collector A from the fuel tank using a pump. The fuel vapor is supplied to a reactor installed in solar collector B. The reactor is filled with a reforming catalyst. If the fuel vapor contacts the reforming catalyst, it will be reformed into gas with a high hydrogen content. Surplus water and CO are contained in the reformed gas. Therefore, water is removed using a gas cooler. Moreover, reformed gas is supplied to a shift unit and a CO oxidation unit, and the amount of CO is oxidized. CO included in the compressed hydrogen is also oxidized using the CO oxidation unit.

(2) Reaction temperature and chemical reaction heat

Figure 1 (b) shows the relationship between the chemical reaction heat and the goal response temperature in each component of the system. The shifter, the gas cooler, the CO oxidation, and the PEFC are accompanied by an exothermic reaction. On the other hand, the vaporizer and the reformer are accompanied by an endothermic reaction. The amount of endothermals of the vaporizer and the reformer of the FBSR is supplied by the solar collectors. After supplying the exhaust heat of the gas cooler, the CO oxidation, and the PEFC to a heat storage tank, the heat is supplied to the demand side. The boiler is operated when there is less thermal storage than demand.

2.3 Electric power system

If reformed gas is supplied to the PEFC, direct-current power will be obtained. This power is supplied to the DC-DC converter, the DC/AC converter, and the inverter, and the power and the frequency of regulation are supplied to the demand side. When there are less power outputs of the fuel cell than the quantity required, the power is supplied to the demand side from the commercial power.

2.4 Loss and auxiliary-machinery power

Fig. 1 (c) is a chart showing the efficiency and conversion rate of all of the components of the FBSR. The conversion rates for the reforming reaction (ψ_r), CO oxidation reaction (ψ_{co}), and hydrogen burning (ψ_{H_2}) are provided. Section 4.2.3 describes the generation efficiency (η_{fc}) of the PEFC. On the other hand, in the analysis in this paper, auxiliary-machinery power of blowers and the pump is not included. The setting value of η_{st}, η_{bl}, η_{dc}, and η_{it} are described in a later section.

2.5 Operation method of the system

When fuel is supplied to vaporizer, the fuel gas is fed to the reforming component. Reformed gas is supplied to the shift unit and the gas cooler, and is stored using cylinder. In order to store hydrogen, the storage tank of the reformed gas is installed in the system. While compressing and storing the reformed gas, it removes the water vapor in the gas using a cooler. Reformed gas is fed to the CO oxidation unit from the cylinder or the gas cooler, and is supplied to the fuel cell. To output power to the commercial power grid (with a regular frequency and voltage), the output of the fuel cell is converted with a DC-DC converter and an inverter. The exhaust heat from the gas cooler, the fuel cell, and the CO oxidization unit is stored. This heat is supplied to the demand side of the FBSR. When supplied solar heat is insufficient, a boiler is operated.

3. Heat transfer analysis

3.1 Efficiency of reforming component

The reforming component shown in Fig. 1 (a) consists of solar collector B and the reactor (Fig. 2 (a)). A reactor end face is a solar insolation acceptance surface with area A_{hs}. Other surfaces are insulated. The solar insolation collected by solar collector B is inputted into the solar insolation acceptance surface. Moreover, the heat input to this solar insolation acceptance surface heats the catalyst layer of the reactor. The efficiency of the reforming component is determined by the ratio of the rate of the higher heating value of the hydrogen produced to that of the amount of condensed solar radiation in solar collectors A and B. Equation (1) is the formula for the efficiency η_s of the reforming component.

$$\eta_s = \frac{\text{The higher heating value of hydrogen } (Q_h)}{\text{Amount of heat collections per day } (Q_A + Q_B)} \tag{1}$$

3.2 Heat transfer in the catalyst layer

The reactor is filled up with several millimeters of the spherical reforming catalyst. In addition, some of solar insolation inputted from the acceptance surface on the reactor is discharged to the ambient air by convection heat transfer q_{con} and radiation heat transfer q_{rad}. Equation (2) is the heat convection of the catalyst layer, and it contains the Damkohler correction number [10]. The value of Da in Eq. (2) is calculated using Eq. (3).

$$Nu = 9.49 \cdot (Re \cdot Pr)^{0.516} \cdot \left(D_c / D_{cl} \right)^{1.43} + 27.2 \cdot Da^{0.325} \tag{2}$$

$$Da = -(H_r \cdot \alpha_r) \cdot D_c / (\rho_g \cdot u_g \cdot C_g \cdot T_g) \tag{3}$$

3.3 Reforming reaction and analytical model for the catalyst layer

The experimental result of ethanol steam reforming using the commercial catalyst by E. Akpan et al., which is shown in Fig. 2 (b), is introduced into the analysis [11]. In this figure, the relationship between the amount of catalyst, the flow rate of ethanol, and the temperature of the catalyst layer and the fuel conversion rate of the catalyst is depicted. The fuel conversion rate increases with an increasing amount of catalyst and with increasing temperature, as shown in Fig. 2 (b). Equation (4) is the two-dimensional heat diffusion equation of the catalyst layer. The temperature of the catalyst layer is represented by T, the coordinates of the direction of the radial direction is represented by r, and the coordinates of the direction of the catalyst layer is represented by x. A surface element is created in the direction of r, and the direction of x, about the catalyst layer of the cylinder type shown in Fig. 2 (a). Figure 2 (c) portrays the element analysis model of the catalyst layer. The element number of the catalyst layer is expressed with $el_{x,r}$ (however, $x = 1,2,...,N_x$, $r = 1,2,...,N_r$).

$$\left(\frac{\partial^2 T}{\partial r^2} + \frac{1}{r} \cdot \frac{\partial T}{\partial r} + \frac{\partial^2 T}{\partial x^2} \right) + q_{\text{r}} = \frac{\rho_{\text{c}} \cdot C_{\text{c}}}{\lambda_{\text{c}}} \cdot \frac{\partial T}{\partial t} \tag{4}$$

Boundary conditions

$$\frac{\partial T}{\partial r} = 0 \qquad \text{at} \quad r = R_{cl},\ 0 \le x \le L_{cl} \tag{5}$$

$$\begin{aligned} -\lambda_{\text{c}} \cdot \frac{\partial T}{\partial x} &= q_s - q_{\text{rad}} - q_{\text{con}} \\ &= q_s - \varepsilon \cdot \sigma \cdot \left(T_{\text{s}}^4 - T_{\infty}^4 \right) - h \cdot (T_{\text{s}} - T_{\infty}) \end{aligned} \tag{6}$$

$$\text{at} \quad x = 0,\ 0 \le r \le R_{cl}$$

$$\frac{\partial T}{\partial x} = 0 \quad \text{at} \quad x = L_{cl}, \quad \frac{\partial T}{\partial r} = 0 \quad \text{at} \quad r = 0$$

$$T = T_{\infty} \quad \text{for} \quad t = 0 \tag{7}$$

$$\frac{\partial}{\partial x} (\rho_{\text{g}} \cdot u_{\text{g}}) = 0 \tag{8}$$

$$\frac{\partial u}{\partial r}=0 \quad \text{at} \quad r=R_{cl}, \quad \frac{\partial u}{\partial x}=0 \quad \text{at} \quad x=L_{cl} \tag{9}$$

$$u=u_0 \quad \text{at} \quad x=0, \quad \frac{\partial u}{\partial r}=0 \quad \text{at} \quad r=0 \tag{10}$$

$$q_{\mathrm{r}}=g_g \cdot \psi_r \cdot H_r \tag{11}$$

3.4 Heat Diffusion Equation

Equation (4) is discretized, and the temperature distribution of the catalyst layer is analyzed under the boundary conditions of Eqs. (5) to (7). The central finite difference method [12] is used to calculate the discretize Eq. (4) in this paper. Here, q_s is the heat concerning the heat exchange wall of the reactor. Equations (5) to (11) are given as the boundary condition when calculating Eq (4). Equation (7) is the boundary condition of temperature and Eq. (8) is the boundary condition of mass flow of process gas. Equations (9) and (10) are the boundary conditions of space velocity. Furthermore, Eq. (11) is the boundary condition of molar flow rate of the process gas. Equation (8) is the mass flow rate of the process gas, and Eqs. (9) and (10) are the boundary conditions in this analysis. The volume flow rate of the process gas is u_g in Eq. (8), and ρ_g is the mean density. The value u_0 in Eq. (10) is the space velocity of the fuel vapor at the entrance of the catalyst layer. This value is the result of dividing the volume flow rate of the fuel vapor by the cross section of the catalyst layer. Equation (11) expresses endothermals from the reforming reaction. Variables g_g, ψ, and H_r in Eq. (11) express the molar flow rate of process gas, the conversion ratio, and the reaction heat, respectively. If the temperature T of the catalyst layer is known, the conversion rate ψ can be obtained from the characteristic of the catalyst. Because H_r is determined by the reforming reaction, if g_g is given, the amount of endothermals q_{r} can be calculated using the reforming reaction.

4. Analysis method

4.1 Temperature distribution of the catalyst layer, and the composition distribution

The temperature distribution ($T_{x,r}$) of the catalyst layer shown in Fig. 2 (c) is obtained by introducing calculus of finite differences into Eq. (4). The boundary conditions at this time are shown in Eq. (5) to Eq. (10). The Gauss Seidel method is used for convergence calculation of the calculus of finite differences. If the temperature distribution $T_{x,r}$ is decided, the conversion rate ($\psi_{x,r}$) in the each element is obtained based on the relationship between catalyst temperature and conversion rate (Fig. 2 (b)). The amount of endothermals of process gas ($q_{r,x,r}$) is calculated based on the value of $\psi_{x,r}$. The temperature distribution ($T_{x,r}$) of the catalyst layer is calculated from these results, and this calculation is repeated to convergence of the discretization equation of Eq. (4).

4.2 Amount of exhaust heat

4.2.1 Gas cooler

The exhaust heat of the gas cooler is calculated using Eq. (12) where the number of components in the process gas is N_g and Δt is the difference in temperature between the process gas in the gas cooler entrance and exit. C_n and G_n are the specific heat and mass flow rates of the gas composition n.

$$H_{gc} = \Delta t \cdot \sum_{n=1}^{N_g} (C_n \cdot G_n) \tag{12}$$

4.2.2 CO oxidation unit

In the CO oxidation unit, the CO concentration is reduced by CO burning. However, the hydrogen contained in the process gas in the case of CO burning may also burn. This selectivity is decided by control of the catalyst temperature. In reality, some of the hydrogen also burns under strict temperature control. In this paper, the rate of hydrogen burning in the process gas is set at 3 %. The exhaust heat of the CO oxidation unit is calculated using Eq. (13). Here, V is the volume flow rate of each gas and J is the calorific value.

$$H_{ox} = V_{CO} \cdot J_{CO} + 0.03 \cdot V_{H_2} \cdot J_{H_2} \tag{13}$$

4.2.3 PEFC

When a PEFC of small capacity compared to the power demand amount is introduced, the operation time of a full load is long. Generally, the exhaust heat power of a PEFC differs with load factor. The PEFC in this paper has many full-load operation hours because the capacity is small compared to the power demand. The PEFC often has to operate with a high load factor. Therefore, the generation efficiency (η_{fc}) of the PEFC is set as 65 %. On the other hand, the exhaust heat of the PEFC is calculated to be 30% of the calorific power of supply hydrogen.

5. Operation case

5.1 Specification of the reforming component

(1) Catalyst layer

The FBSR was introduced into individual houses in Sapporo, Japan. The specification of the reforming component introduced into this case analysis is described in Table 1 (a). The diameter of the catalyst layer D_{cl} is 80 mm and its width L_{cl} is 60 mm. The reactor is filled up with the reforming catalyst of 3 mm average particle diameter. The catalyst filling factor is 0.85. The detailed experimental results of the ethanol steam reforming by this reforming catalyst are described by reference 6. In addition, the catalyst layer is divided into elements of 2 mm length in the directions of r and x. The numbers of elements are $N_x = 30$ and $N_r = 40$.

(2) Heat system

The heat transfer coefficient h_∞ of the convective heat transfer q_{con} described by Section 3.2 was set at 10 W/m^{2}K (natural convection). Moreover, ε_{hs} of the radiation heat transfer q_{rad} gives 0.95 assuming a black body. The area A_{hs} on the solar insolation acceptance surface of the reactor is 0.005 m^2. The transmissivity of the heat exchange wall of the reactor was set at 0.9, and the condensing efficiency of the solar collector was set at 90%.

(3) Solar collector and fuel supply

In the analysis in this paper, the collecting area of solar collector A and solar collector B were both set to be 1 m^2 (unit area). In the convergence calculation of the discretization equation, an analytical accuracy of 10^{-5} was used. The use of an ethanol solution fuel supply determined that the value of the horizontal axis in Fig. 2 (b) (Amount of catalysts /Ethanol flow rate) is 35000 kg/(kmol/s).

5.2 Storage of the reformed gas

The reformed gas can be compressed and stored in the FBSR (broken-line block in Fig. 1 (a)). Accordingly, the reformed gas with the pressure P_0 and the flow rate $U_{0,t}$ outputted from the gas

cooler is pressurized to P_{cp} with a compressor. Here, the subscript t is sampling time. The work $W_{p,t}$ of the compressor is assumed to be the work of compression by an ideal gas and is calculated using Eq. (14). The compressor efficiency η_{cp} in the equation includes the electricity consumption in an electric motor, the transmission loss of power, loss due to insufficient air leak and cooling, and other mechanical loss.

$$W_{p,t} = P_0 U_{0,t} \ln\left(P_{cp}/P_0\right)/\eta_{cp} \tag{14}$$

5.3 Installation requirements of the system and demand characteristic

The operation of the power and heat in the case of introducing the FBSR into standard houses in Sapporo is planned. However, since a detailed report about the operation method of this power has already been published [8], this paper focuses on examining the overall efficiency of the system.

The power load and the heat consumption of a house in Sapporo on a representative day in both March (March 1) and August (August 23) are shown in Figs. 3 (a) and (b) [13]. Because Sapporo is located in a cold district, there is no cooling load in August. On the other hand, the space heating load in March is supplied from the exhaust heat of the system and the backup boiler. As shown in Fig. 3, the characteristics concerning the amount of solar radiation and outside air temperature [14] will differ greatly in March and August. In this paper, as observational data of the solar irradiance and the outside air temperature, Surface-Weather-Observation 1-Minute Data and 2007 Sapporo District Meteorological Observatory and Japan Meteorological Business Support Center [14] are used. The figure at the bottom of Fig. 3 depicts daylight hours on each representative day. The amount of solar radiation, outside air temperature, and daylight hours are data collected at 1-minute intervals.

6. Results and discussion

6.1 Temperature distribution of the catalyst layer

Figure 4 shows the result of the transient response characteristic of the catalyst layer temperature when inputting constant solar insolation (250 W/m^2, 500 W/m^2, 1000 W/m^2) into the reactor [8]. In Fig. 4, 0 s is the stable time of the acceptance surface temperature after inputting solar insolation into the reactor. When the outside air temperature is 293 K, the acceptance surface with solar irradiance of 250 W/m^2 rises to about 500 K. In the input of 1000 W/m^2, the acceptance surface rises to about 890 K. The conversion rate of ethanol steam reforming increases, which leads to a high catalyst temperature in the reactor. Therefore, the temperature distribution of the catalyst layer shown in Fig. 4 differs so greatly that solar irradiance is large.

6.2 Composition of the process gas

Figure 5 shows the analysis result of the process gas composition of the catalyst layer when inputting constant solar insolation (250 W/m^2 and 500 W/m^2) into the reactor [8]. This figure shows the process gas composition along the x axis of the catalyst layer as predicted by the analysis. This figure shows the composition of each gas with its respective molar flow rate. The molar flow rate of hydrogen is larger than other gases in the composition. Distribution of the molar flow rate of hydrogen, and the time at which the hydrogen flow rate becomes stable are influenced by the magnitude of the solar irradiance input into the reactor. If there is little solar irradiance and there a short period of solar radiation fluctuation, the hydrogen generation rate may not reach the maximum possible. From this result, when there is short-time fluctuation solar radiation with little

solar irradiance, the hydrogen generating rate may not reach a stable generation rate (rated speed) by a response delay.

6.3 Amount of hydrogen generated

Figure 6 shows the analysis result of the amount of hydrogen generated by the FBSR using the amount of solar radiation, outside air temperature, and daylight hours shown in Fig. 3. The hydrogen generating rate fluctuates a lot when comparing August 23 to March 1. As shown in Fig. 3, from 6:00 a.m. to 11:00 a.m., the solar insolation fluctuation on the representative day in March is stable compared to that in August. The cause of this solar insolation fluctuation is a shadow by clouds. As a result, in Fig. 6, the amount of hydrogen production on a representative morning in March will be stabilized compared with that in August. As shown in Fig. 4, the rate of hydrogen generation may not be less than rated output in a weather condition with solar insolation fluctuation.

6.4 Production of electricity and amount of purchased powers

Figure 7 shows the analysis result of the production of electricity of the FBSR and the amount of purchased powers. In this analysis, the power is purchased when the production of electricity of the FBSR is less than the power demand amount shown in Fig. 3. As for the result of Fig. 7, the solar irradiance on the representative day of each month and the characteristic of the outside air temperature affect the purchase power. Moreover, when introducing solar collector A and solar collector B with areas of 1.0 m^2, the power load peak at 8:00 of both representative days (Fig. 3) can be decreased. However, in order to decrease the peak around 19:00, the increase in the compressed hydrogen by extension of solar collecting area is required. Moreover, a time shift of the electric power supply is required using hydrogen storage equipment. When the amount of production of the reformed gas by solar collectors A and B is introduced into the power load pattern shown in Fig. 3, storage of the reformed gas is not required. The electric power supply rate of the FBSR to a power demand amount is predicted to be 21.4% and 25.3% on a representative day in March and August, respectively.

6.5 Operation of the exhaust heat

Figures 8 and 9 show the analysis result of the exhaust heat of the fuel cell, the CO oxidation unit, the gas cooler, and the heat of the backup boiler on representative days in March and August. In terms of the solar insolation fluctuation from 6:00 a.m. to 11:00 a.m., the exhaust heat power of the morning in March is stable compared to that in August. This is due to the difference in solar insolation fluctuation on a representative day in each month shown in Fig. 3. The heat supply rates of the FBSR to heat demand is predicted to be 1.2% and 13.7% on the representative day in March and August (except for boiler power).

6.6 Overall efficiency

The conversion rates to the electric power are 30.7% (March representative day) and 27.1% (August representative day) every month among the solar irradiance obtained by the 1 m^2 solar collectors A and B on the representative days. On the other hand, the conversion rates to heat supply of solar irradiance are 16.7% (March representative day) and 14.8% (August representative day). Therefore, the overall efficiency of the FBSR by this operation case is 47.4% (March representative day) and 41.9% (August representative day). The difference in solar irradiance will be 1.32 times in August compared with that on the March representative day. However, the overall

efficiency on the March representative day is larger than that in August. Therefore, the magnitude and the number of occurrences of the solar insolation fluctuation strongly influence the overall efficiency.

7. Conclusions

The overall efficiency of a PEFC with the bioethanol reforming system using a sunlight heat source (FBSR) was investigated by numerical analysis. In this paper, the heat transmission characteristics of the catalyst layer installed in the reactor were investigated. The transient characteristic of hydrogen generation was examined based on these results. Furthermore, the supply and amount of purchase of electric power and heat were investigated using the energy-demand characteristic in a standard house in addition to meteorological data on representative days in March and August in Sapporo, Japan. The total collecting area of the solar collectors was 2 m^2. The following conclusions were drawn from these analysis results. As uncertainty in this analysis, the calculation error, the setting performance of each equipment, etc. can be considered. Magnitude of these influences and error concerning the grid system is explained by future study.

(1) The magnitude of solar irradiance greatly influences the temperature distribution and composition distribution of process gas in the catalyst layer. When there is short-time fluctuation solar radiation with little solar irradiance, the hydrogen generation rate may not reach a stable generation rate (rated speed) by a response delay.

(2) The rate of converting sunlight into electrical power in the proposed system is 30.7% and 27.1% on representative days in March and August, respectively. On the other hand, the rate converted into heat is 16.7% and 14.8%, respectively. As a result, the overall efficiency of the FBSR by the analysis case in this paper is 47.4% and 41.9%, respectively. These results indicate that the proposed system is competitive with other energy systems, such as a photovoltaic cell. However, operation of the FBSR takes the cost of the bioethanol.

Nomenclature

C : Specific heat J/(g・K)
Da : Modified Damkohler number
el : The element number of the catalyst layer
G : Mass flow rate g/s
g_g : Molar flow rate mol/s
H : Reaction heat J/mol
h : Heat transfer coefficient W/(m^2・h・K)
J : Calorific value J/m^3
L : Length, width m
N : The number of elements
N_g : The number of gas composition
Nu : Nusselt number
P : Power W
P_0 : Inlet pressure of the process gas Pa
P_{cp} : Outlet pressure of the process gas Pa
Pr : Prandtl number
Q : Quantity of heat J

q : Heat W

R : Radius m

r : Radial direction of the catalyst layer

Re : Reynolds number

T : Temperature K

t : Sampling time s

Δt : Temperature difference K

U_0 : The volume flow rate of the process gas m^3/s

u : Flow rate m/s

u_0 : Initial flow rate m/s

W_p : Work of the compressor W

x : Axial direction of the catalyst layer

Greek Symbols

α_r : Reaction rate $mol/(m^3 \cdot s)$

χ : Layer of the element

ε : Emissivity

η : Efficiency

η_{cp} : Efficiency of the compressor

η_s : Efficiency of the reforming component

λ : Heat conductivity $W/(m \cdot K)$

ρ : Density g/m^3

σ : Stefan-Boltzmann constant

ψ : Conversion ratio

Subscripts

A , B : Solar collectors A and B

bl : Boiler

c : Catalyst

cl : Catalyst layer

con : Convective heat transfer

cf : CO oxidation unit to the cell stack

cm : Customer

con : Convection

cp : Commercial power

dc : DC-DC converter

fc : Cell stack

g : Process gas

gc : The gas cooler to the heat storage tank

h : The higher heating value of hydrogen

hs : Heat supply surface of the reactor

it : DC-AC converter and inverter

ox : The CO oxidation unit

pv : The pump to the vaporizer

r : Reforming

rad : Radiation
rs : The reactor to the shift unit
s : Sunlight
sc : The gas cooler to the CO oxidation unit
st : Storage tank
sg : The shift unit to the gas cooler
tb : The fuel tank to the boiler
∞ : Ambient air

Acknowledgement

This work was partially supported by a Grant-in-Aid for Scientific Research (C) from JSPS.KAKENHI (20560204).

References

(1) Shin-ya OBARA and Itaru TANNO, Development of Distributed Energy System due to Bio-ethanol PEM Fuel Cell with Solar Reforming, Part 1—Evaluation of Basic Performance, Transactions of the Society of Heating, *Air-Conditioning and Sanitary Engineers of Japan*, 123, (2007), 23-32.

(2) Shin-ya OBARA and Itaru TANNO, Development of Distributed Energy System due to Bio-ethanol PEM Fuel Cell with Solar Reforming, Part 2—High-speed analysis of the operation plan using a neural network, *Transactions of the Society of Heating, Air-Conditioning and Sanitary Engineers of Japan*, 130, (2008), 33-42.

(3) Shin-ya OBARA and Itaru TANNO, Operation Prediction of a Bioethanol Solar Reforming System Using a Neural Network, *Journal of Thermal Science and Technology*, Vol. 2, No. 2, 2007, 256-267.

(4) Abdul-Majeed Azad, Sathees Kesavan, Sirhan Al-Batty, A Closed-Loop Proposal for Hydrogen Generation Using Steel Waste and a Prototype Solar Concentrator, *International Journal of Energy Research*, Vol. 33, No. 5, 2009, 481-498.

(5) Adam Noglik, Martin Roeb, Christian Sattler, Robert Pitz-Paal, Experimental Study on Sulfur Trioxide Decomposition in a Volumetric Solar Receiver-reactor, *International Journal of Energy Research*, 2009, Early View.

(6) John Turner, George Sverdrup, Margaret K. Mann, Pin-Ching Maness, Ben Kroposki, Maria Ghirardi, Robert J. Evans, Dan Blake, Renewable Hydrogen Production, *International Journal of Energy Research*, Vol. 32, No. 5, 2008, 379-407.

(7) Patrice Charvin, Abanades Ste´phane, Lemort Florent, Flamant Gilles, Analysis of solar chemical processes for hydrogen production from water splitting thermochemical cycles, *Energy Conversion and Management*, Vol. 49, 2008, 1547–1556.

(8) Fernando Fresno, Rocío Fernández-Saavedra, M. Belén Gómez-Mancebo, Alfonso Vidal, Miguel Sánchez, M. Isabel Rucandio, Alberto J. Quejido and Manuel Romero, Solar hydrogen production by two-step thermochemical cycles: Evaluation of the activity of commercial ferrites, *International Journal of Hydrogen Energy*, Vol. 34, No. 7, 2009, 2918-2924.

(9) Jin Xuan, Michael K.H. Leung, Dennis Y.C. Leung, Meng Ni, A review of biomass-derived

fuel processors for fuel cell systems, *Renewable and Sustainable Energy Reviews*, Vol. 13, No. 6-7, 2009, 1301-1313.

(10) Y. Usami, S. Fukusako and M. Yamada, Heat and Mass Transfer in a Reforming Catalyst Bed (Quantitative Evaluation of the Controlling Factor by Experiment), *Transactions of the JSME*, Series B, 67(659), (2000), 1801-1808.

(11) E. Akpan, A. Akande, A. Aboudheir, H. Ibrahim and R. Idem, Experimental, Kinetic and 2-D Reactor Modeling for Simulation of the Production of Hydrogen by the Catalytic Reforming of Concentrated Crude Ethanol (CRCCE) Over a Ni-Based Commercial Catalyst in a Packed-Bed Tubular Reactor, *Chemical Engineering Science*,62(12), (2007), 3112-3126.

(12) Mitchell, Andrew Ronald, *Finite Difference and Related Methods for Differential Equations*. Wiley: New York, 2001.

(12) K. Narita, *The Research on Unused Energy of the Cold Region City and Utilization for the District Heat and Cooling*, Ph.D. thesis, Hokkaido University. (1996).

(13) *Surface-weather-observation 1-minute data, 2007 Sapporo district meteorological observatory*, Japan Meteorological Business Support Center, (2008), Tokyo.

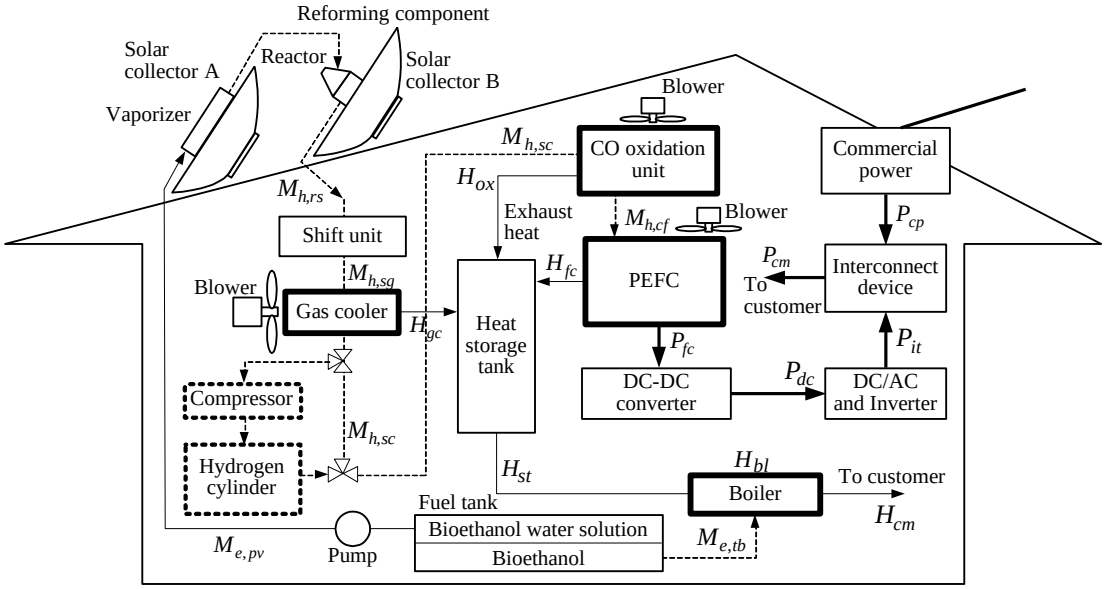

(a) Block diagram

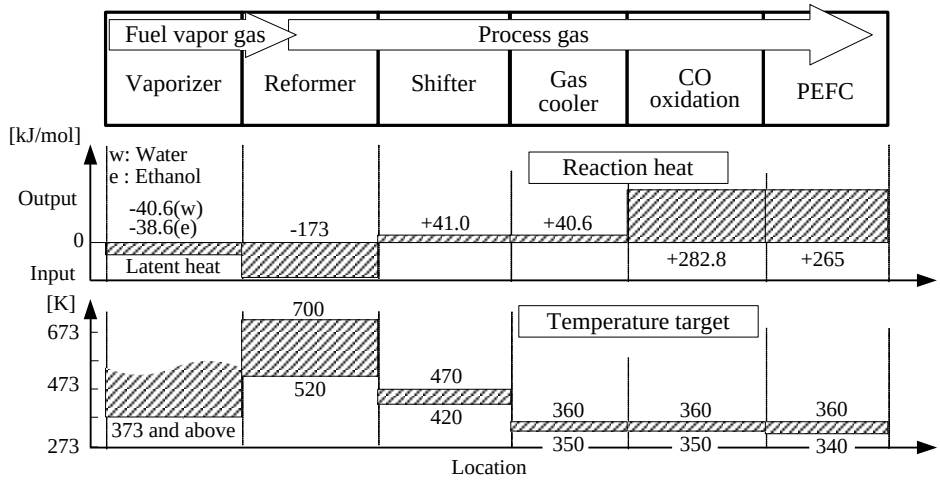

(b) Reaction heat and temperature target

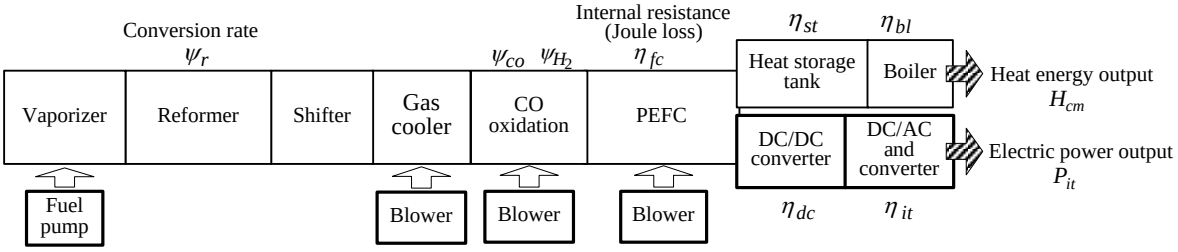

(c) Loss of power and heat

Fig. 1 System design

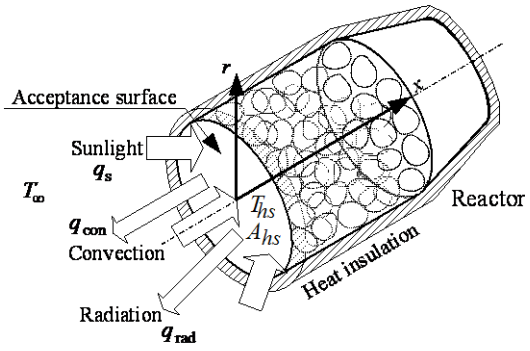

(a) Reactor

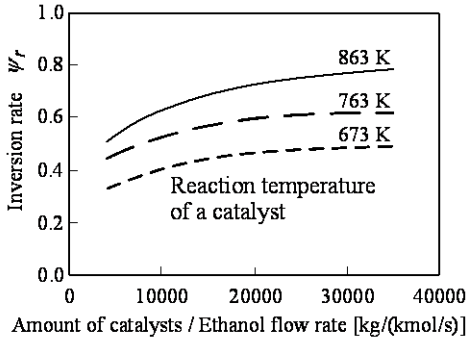

(b) Catalyst performance [6]

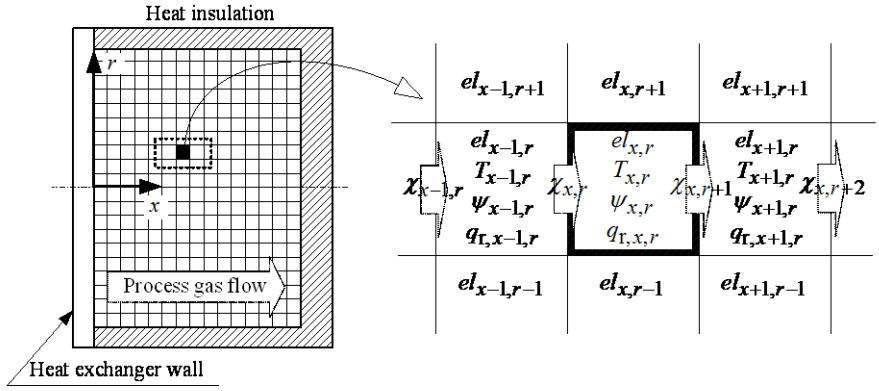

(c) Analysis of the heat transfer

Fig. 2 Reactor

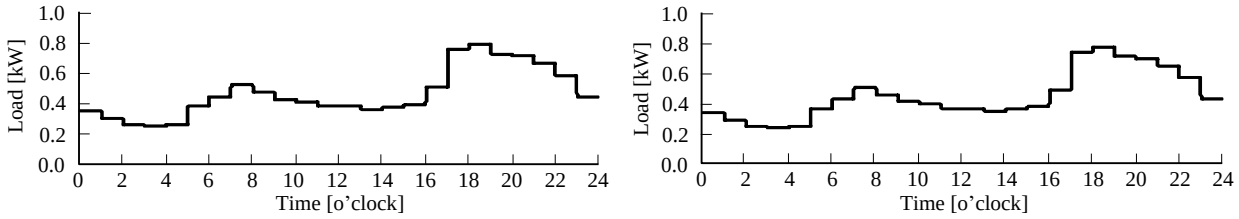

Power load

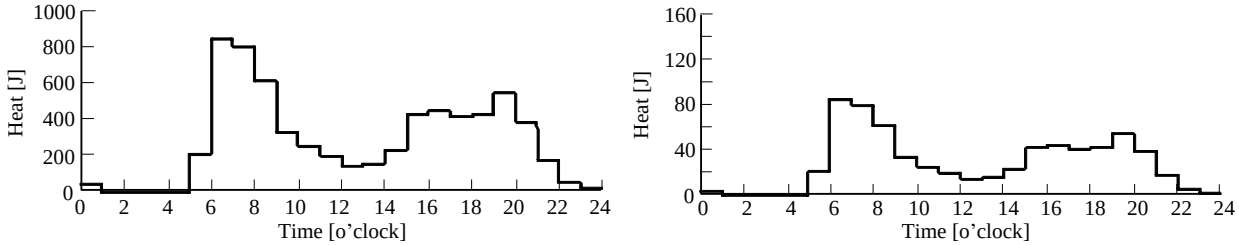

Heat consumption

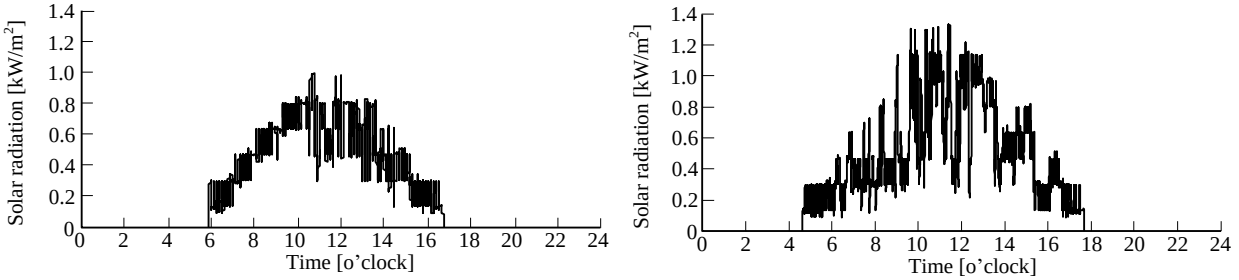

The amount of solar radiation 1-minute data

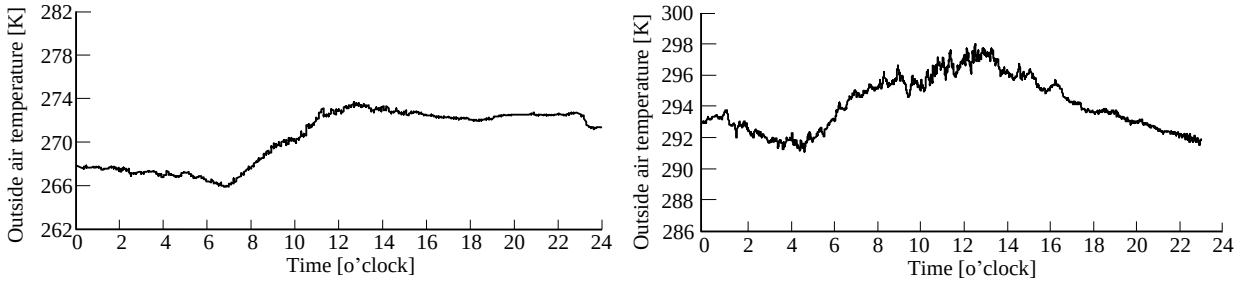

Outside air temperature Is 1-minute data

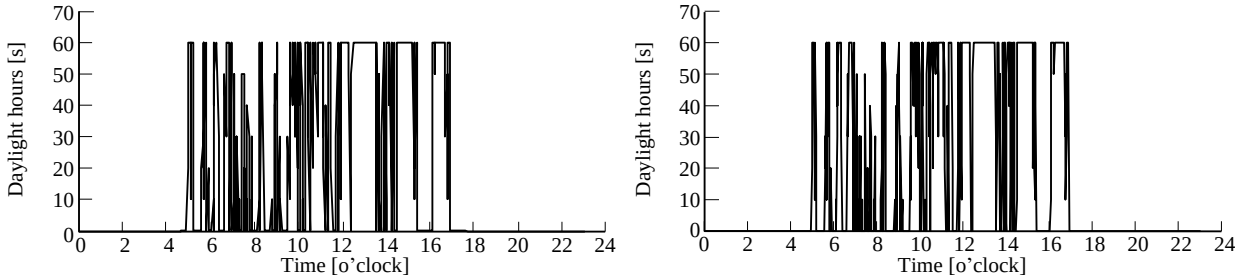

Daylight hours 1-minute data

(a) March 1, 2007 (b) August 23, 2007

Fig. 3 Weather observation 1-minute data in Sapporo

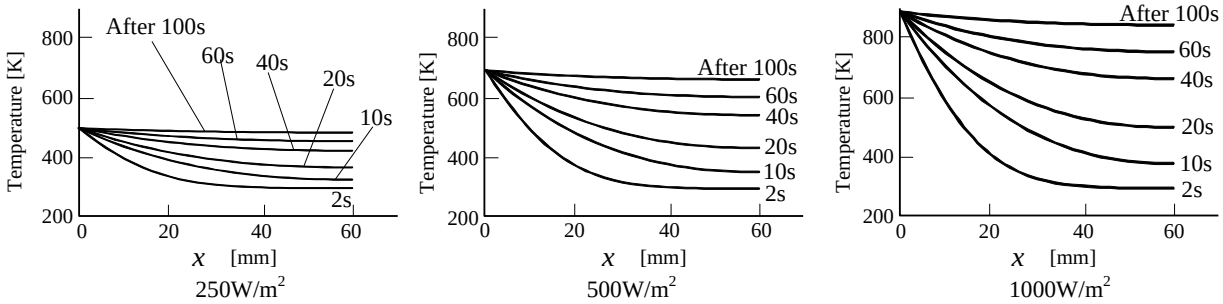

Fig. 4 Temperature distribution in the catalyst layer of the reactor

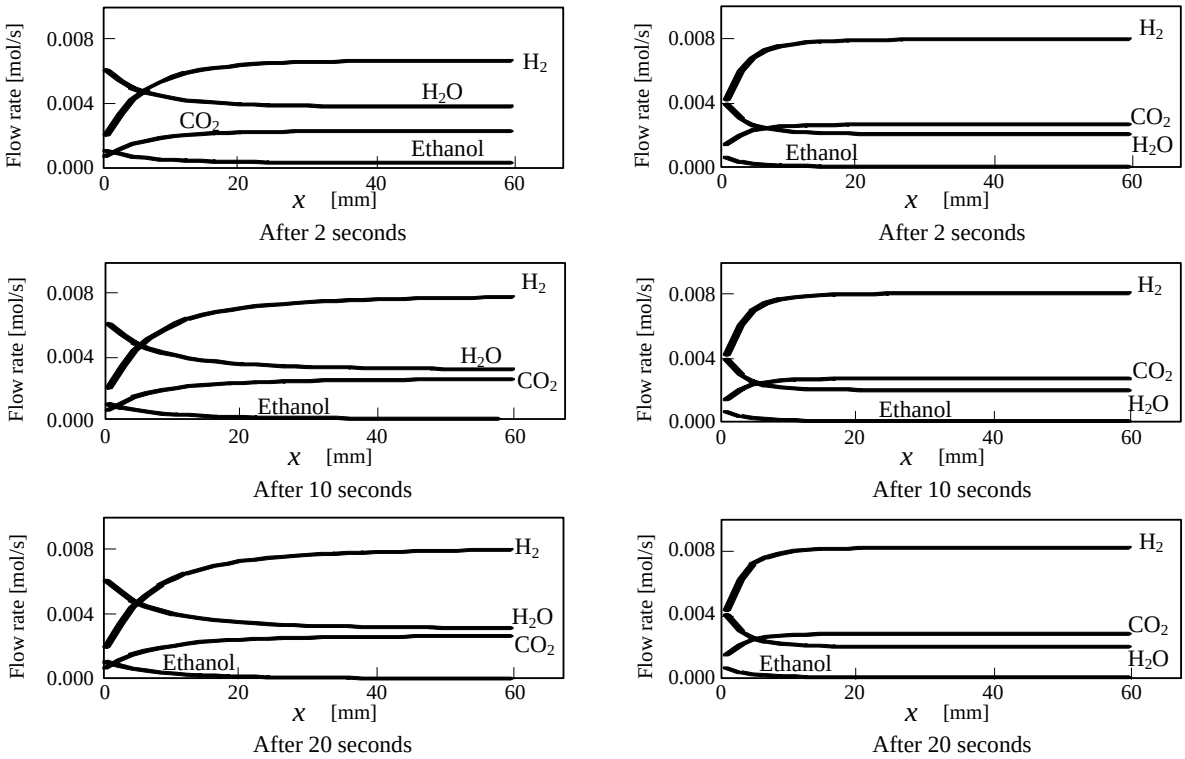

(a) The amount of heat collection of solar collector B is 250W/m^2

(b) The amount of heat collection of solar collector B is 500W/m^2

Fig. 5 Flow rate of process gas in the catalyst layer. Outside air temperature is 293 K.

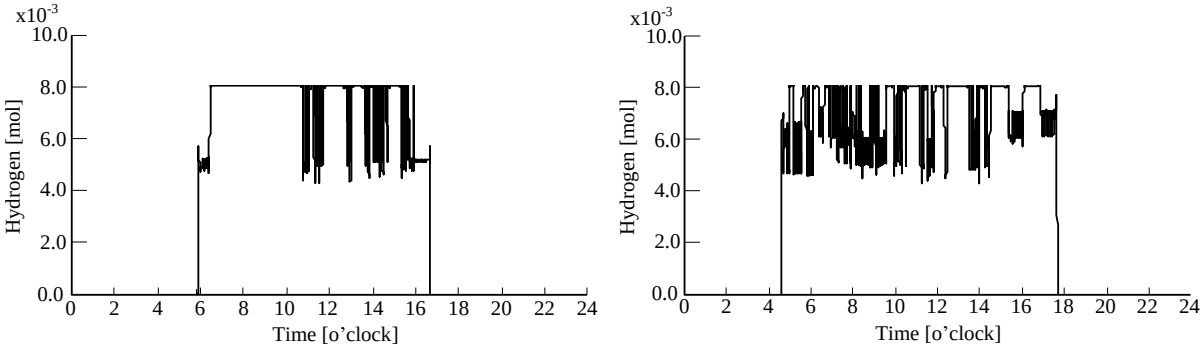

(a) March 1, 2007 (b) August 23, 2007

Fig. 6 Characteristics of the hydrogen flow rate of the FBSR

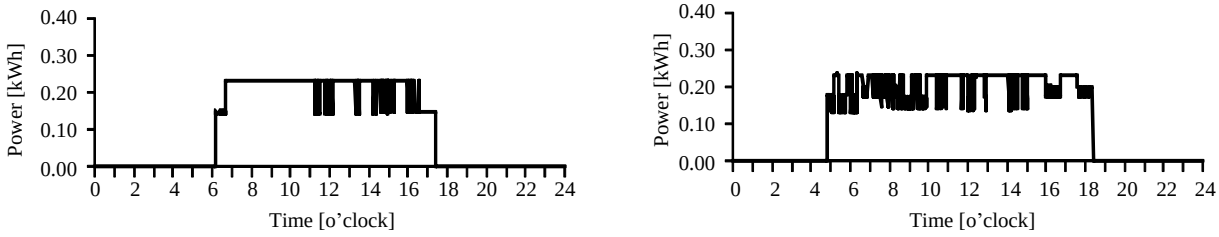

Power output from the FBSR

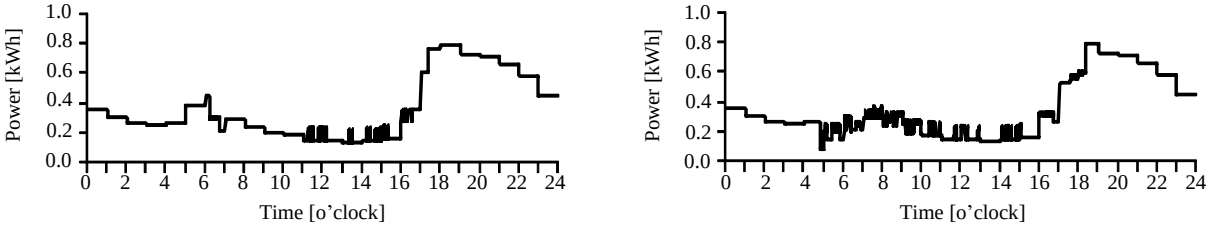

Purchase power

(a) March 1, 2007. (b) August 23, 2007.

Fig. 7 Analysis results of the power operation plan

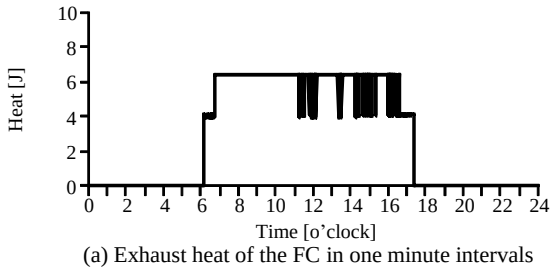

(a) Exhaust heat of the FC in one minute intervals

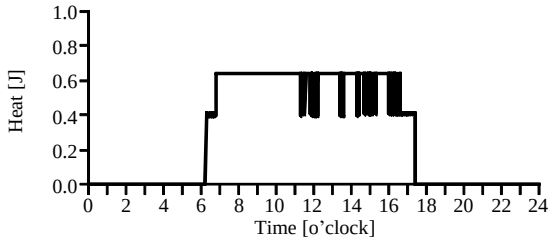

(b) Exhaust heat of the CO oxidation unit in one minute intervals

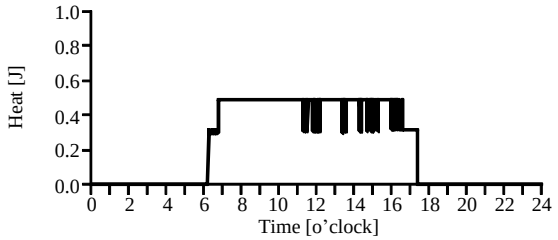

(c) Exhaust heat of the gas cooler in one minute intervals

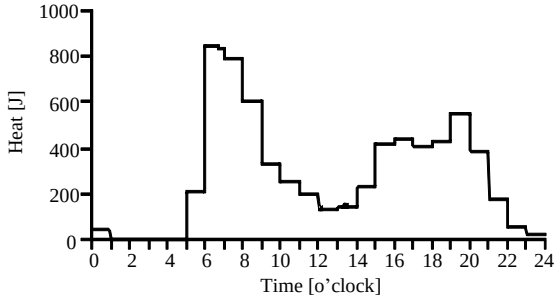

(d) Purchased heat in one minute intervals

Fig. 8 Analysis results of the heat operation plan on March 1, 2007.

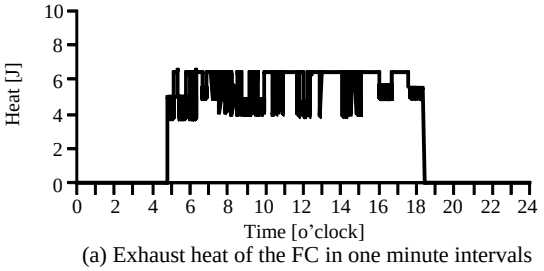

(a) Exhaust heat of the FC in one minute intervals

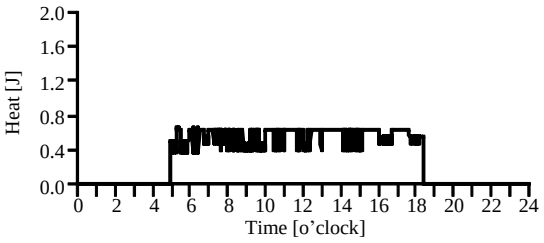

(b) Exhaust heat of the CO oxidation unit in one minute intervals

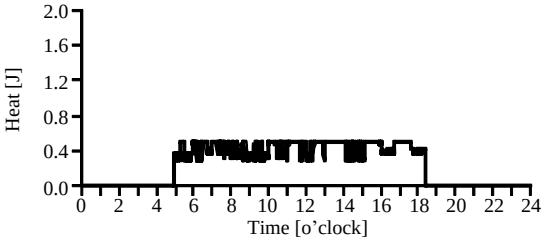

© Exhaust heat of the gas cooler in one minute intervals

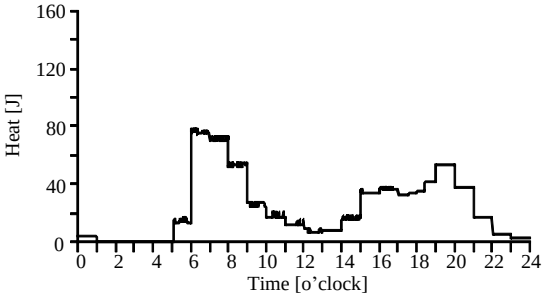

(d) Purchased heat in one minute intervals

Fig. 9 Analysis results of the Heat Operation plan on August 23, 2007.

Table 1 Analysis condition

Each concentration area of the solar collector A and B	1.0 m^2
Reactor	
Length of the catalyst layer (L_{cl})	60 mm
Diameter of the catalyst layer (D_{cl})	80 mm
Particle diameter of the catalyst (D_c)	3.0 mm
Steam/carbon ratio	3.0
Catalyst filling factor	0.85
Sampling time	0.01 s
The number of element of *x*-axis (N_x)	30
The number of element of *r*-axis (N_r)	40
Density of the catalyst	213 kg/m^3
Heat conductivity of the catalyst	10 W/mK
Efficiency	
DC-DC converter (η_{dc})	95 %
DC-AC converter and inverter (η_{it})	95 %
Boiler (η_{bl})	90 %
Heat storage (η_{st})	90 %
Loss of the CO oxidation unit	3 %

Table 2 Analysis results of the FBSR performance

	March 1	August 23
Aamount of solar radiation per day by the solar collectors A and B	28.0 MJ/Day	37.0 MJ/Day
Amount of hydrogen production per day	100 g/Day	117 g/Day
Efficiency of a reforming component (The higher calorific value of hydrogen / amount of heat collections per day)	47 %	42 %
Amount of power demand per day	11.16 kWh	11.03 kWh
Amount of power generation per day	2.39 kWh	2.79 kWh
Amount of CO_2 emissions per day	732 g/Day	854 g/Day
Use rate of renewable energy (Condensing area 2.0 m^2)		
Power	30.7%	27.1 %
Heat	16.7 %	14.8 %
Total	**47.4 %**	**41.9 %**
System output to the quantity power demanded	21.4 %	25.3 %
System output to the quantity heat demanded (except for the boiler)	1.2 %	13.7 %

Captions

Fig. 1 System design
(a) Block diagram
(b) Reaction heat and temperature target
(c) Loss of power and heat

Fig. 2 Reactor
(a) Reactor
(b) Catalyst performance [6)]

Fig. 3 Weather observation 1-minute data in Sapporo
(a) March 1, 2007
(b) August 23, 2007

Fig. 4 Temperature distribution in the catalyst layer of the reactor

Fig. 5 Flow rate of process gas in the catalyst layer. Outside air temperature is 293 K.
(a) The amount of heat collection of solar collector B is 250 W/m^2
(b) The amount of heat collection of solar collector B is 500 W/m^2

Fig. 6 Characteristics of the hydrogen flow rate of the FBSR
(a) March 1, 2007
(b) August 23, 2007

Fig. 7 Analysis results of the power operation plan
(a) March 1, 2007.
(b) August 23, 2007.

Fig. 8 Analysis results of the heat operation plan on March 1, 2007.
(a) Exhaust heat of the FC in one minute intervals
(b) Exhaust heat of the CO oxidation unit in one minute intervals
(c) Exhaust heat of the gas cooler in one minute intervals
(d) Purchased heat in one minute intervals

Fig. 9 Analysis results of the Heat Operation plan on August 23, 2007.
(a) Exhaust heat of the FC in one minute intervals
(b) Exhaust heat of the CO oxidation unit in one minute intervals
(c) Exhaust heat of the gas cooler in one minute intervals

(d) Purchased heat in one minute intervals

Table 1 Analysis condition

Table 2 Analysis results of the FBSR performance